Complex behavior in driven unidirectionally coupled overdamped Duffing elements

Visarath In,[1,*] Antonio Palacios,[2,†] Adi R. Bulsara,[1,‡] Patrick Longhini,[1] Andy Kho,[1] Joseph D. Neff,[1] Salvatore Baglio,[3] and Bruno Ando[3]

[1]*Space and Naval Warfare Systems Center, Code 2373, 49590 Lassing Road, A341, San Diego, California 92152-5001, USA*

[2]*Nonlinear Dynamics Group, Department of Mathematics & Statistics, San Diego State University, San Diego, California 92182, USA*

[3]*Dipartimento di Ingegneria Elettrica Elettronica e dei Sistemi, Università degli Studidi Catania, Viale A. Doria 6, 95125 Catania, Italy*

(Received 28 March 2006; published 19 June 2006)

It is well known that overdamped unforced dynamical systems do not oscillate. However, well-designed coupling schemes, together with the appropriate choice of initial conditions, can induce oscillations (corresponding to transitions between the stable steady states of each nonlinear element) when a control parameter exceeds a threshold value. In recent publications [A. Bulsara *et al.*, Phys. Rev. E **70**, 036103 (2004); V. In *et al.*, *ibid.* **72**, 045104 (2005)], we demonstrated this behavior in a specific prototype system, a soft-potential mean-field description of the dynamics in a hysteretic "single-domain" ferromagnetic sample. These oscillations are now finding utility in the detection of very weak "target" magnetic signals, via their effect on the oscillation characteristics—e.g., the frequency and asymmetry of the oscillation wave forms. We explore the underlying dynamics of a related system, coupled bistable "standard quartic" dynamic elements; the system shows similarities to, but also significant differences from, our earlier work. dc as well as time-periodic target signals are considered; the latter are shown to induce complex oscillatory behavior in different regimes of the parameter space. In turn, this behavior can be harnessed to quantify the target signal.

DOI: 10.1103/PhysRevE.73.066121 PACS number(s): 02.50.Ey, 05.10.−a, 85.25.Dq

I. INTRODUCTION

Well-designed coupling schemes, together with an appropriate choice of initial conditions, can induce oscillations (i.e., periodic transitions between stable attractors) in overdamped dynamical systems when a control parameter exceeds a threshold value [1]. We have demonstrated this behavior in a specific prototype system, three unidirectionally coupled ferromagnetic cores, the basis of a coupled core fluxgate magnetometer, subject to a "residence times" readout scheme [2] that is used to detect magnetic flux signals. Our analysis showed that N (taken to be odd, although the oscillatory behavior can also be seen for N large and even) unidirectionally coupled elements with cyclic boundary conditions would, in fact, oscillate when a control parameter—in this case the coupling strength—exceeded a critical value. Note that energy conservation dictates that at least one of the elements must have an initial state different from the others for the oscillations to occur. The oscillations (corresponding, in this case, to switching events between the stable magnetization states of each core) have been exploited to detect very weak "target" dc and time-varying magnetic signals via their effect on the oscillation characteristics. It is important to stress that this behavior is quite general; in fact, it has been applied to analyses of the frequency-selective properties of interacting neural networks [3,4]. The emergent oscillations, which can be controlled by adjusting the system parameters, open up new possibilities for the exploitation of a large class of (normally) nonoscillatory systems for a variety of practical applications that involve the use of emergent oscillations as a reference.

In [1], we considered a system of coupled elements having "soft"-potential dynamics, characteristic of hysteretic single-domain ferromagnetic cores. This work has led to exploiting the emergent oscillatory behavior for signal detection purposes: specifically, an external symmetry-breaking dc magnetic signal having small amplitude (usually much smaller than the energy barrier height of a single element) can be detected and quantified via its effect on the oscillation frequency and asymmetry of the oscillation wave forms. In the presence of a weak *subthreshold* time-periodic target signal, a richness of frequency-locking behavior has been observed [5] in the coupled-core fluxgate magnetometer; in turn, this behavior is being used for the classification of time-dependent target magnetic signals through analyses of their frequency content. It must be noted that the above-described system is somewhat unique. The macroscopic dynamics of each ferromagnetic core are underpinned by a mean-field description that can be derived in the continuum limit of a simple discrete spin model [6]. This results in the coupling and interaction terms in the dynamics of each coupled element being highly nonlinear, since they are absorbed into the argument of the nonlinearity (in this case the hyperbolic tangent function that is bounded by ±1). This description is not applicable across the board, with most other nonlinear elements describable by the standard dynamics $\dot{x}=-\nabla U(x)+F(t)$ of a macroscopic state variable $x(t)$ subject to a driving force $F(t)$ in a potential energy function $U(x)$. As a prototype or test system, the "standard quartic" functional form $U(x)=-\frac{a}{2}x^2+\frac{b}{4}x^4$ is often employed. Given the functional form $U(y)=\frac{y^2}{2}-\frac{1}{c}\ln\cosh\{c[y+h(t)]\}$ of the dynamics of a single ferromagnetic core having macroscopic magnetization $y(t)$ with an external bias $h(t)$, one expects that there will be a

*Electronic address: visarath@spawar.navy.mil
†Electronic address: palacios@euler.sdsu.edu
‡Electronic address: bulsara@spawar.navy.mil

few similarities but also some marked differences between the x and y dynamics.

In this work we consider a coupled dynamic system whose building blocks are bistable Duffing elements underpinned by the potential $U(x)$ introduced above. The goal is, however, much more than a simple repeat of our previous calculations with a different potential energy function. As already stated, the magnetic interaction is somewhat unique and systems are more likely to follow dynamics of the form given above for the variable $x(t)$. In fact, the x dynamics can be used to describe the response of a ferroelectric sample in the presence of an external electric field E. The variable $x(t)$ is, then, a time-dependent polarization P and the material is known to exhibit a hysteretic P-E transfer characteristic in response to an adiabatic sweep of the electric field intensity E. A coupled version of this system is the backbone of a new class of electric field sensors that are under development. When complete, these sensors are expected to break new ground (compared to existing electric field sensors) insofar as changes in the ambient electric field might be quantified onboard the sensor rather than via a measurement of the potential drop across electrodes implanted in an active (conducting) medium, as is current practice. While the laboratory development of these sensors proceeds (they will be the subject of a future publication) it is, therefore, of considerable interest to examine their dynamics as a function of system control parameters (e.g., the coupling strength) as well as external signal parameters. As already mentioned, the results are likely to be applicable to a broad class of coupled dynamical systems whose elemental dynamics follow the generic form of the x dynamics given above, or some variation thereof (but not necessarily the mean-field-type dynamics of the coupled magnetic elements).

This paper is organized as follows: we begin with a consideration of a unidirectionally coupled, overdamped, three-element Duffing network driven by an external (or "target") dc signal. The threshold conditions for making the system oscillate are derived and the oscillation frequency quantified in terms of the coupling parameter and the target signal. This is followed by the introduction of a time-periodic external target signal, whose presence is seen to lead to a very rich response in the coupled system; as already mentioned, our results are expected to lead to techniques to quantify unknown external signals in detectors based on coupled dynamical elements, wherein the individual elemental dynamics follow the Duffing (or related) paradigm.

II. UNIDIRECTIONALLY COUPLED, OVERDAMPED DUFFING ELEMENTS WITH dc EXTERNAL SIGNAL

We consider a system of N (unidirectionally) coupled bistable overdamped Duffing elements in the presence of a weak (compared to the energy barrier height of a single uncoupled element) dc external target signal ε_0:

$$\tau \dot{x}_i = a x_i - b x_i^3 + \lambda (x_i - x_{i+1}) + \varepsilon_0, \tag{1}$$

where $i = 1, \ldots, N \bmod N$, $x_i(t)$ is a generic-state variable, with the parameters (a,b) characterizing each element, λ being an interelement coupling coefficient (note the absence of bidirectional coupling), and c is a coupling constant (or amplification parameter, depending on the mechanism) to the external target signal. τ is a time constant, usually depending in a complex way on geometrical and physical (material) parameters; it defines (via its inverse) the individual element bandwidth. One realizes, immediately, that the dynamics of the system (1) are likely to be quite different from those discussed in [1] because of the differences in the (interelement as well as external signal) coupling mechanisms, as already discussed in the preceding section.

It is instructive to simply examine the solutions of the system (1) for different parameter values. Assume (a,b) to be fixed and positive, so that the individual elemental dynamics are bistable together with an initial condition that sets at least one of the state variables different from the others at $t=0$. Then, for the coupling coefficient λ below a critical value λ_c (to be determined), the system remains quiescent after a possible short-lived initial transient; the elements settle into one of their stable attractors (potential minima) and remain there for all time, unless an external disturbance (of suitable amplitude) is applied. Above the critical coupling, however, energy is transferred from one element to the other, allowing each element to make transitions between its stable attractors; the resulting "oscillations" are periodic but not sinusoidal. For $\varepsilon_0 = 0$, the oscillations are symmetric; a nonzero target signal renders each potential asymmetric *a priori*; i.e., the potential wells have unequal depth resulting in a difference in residence times in the two attractors for each element. In turn, the oscillations no longer have symmetric (mirror-image) half-cycles, and their period is also changed; as already discussed, these characteristics have already been exploited in a coupled-core fluxgate magnetometer [1] for signal detection and characterization purposes using the (nonspectral) residence times detection technique [1,2]. The above characteristics are well displayed in Fig. 1; in this figure, we have also plotted the summed response $X(t) = \Sigma_i x_i(t)$. We will see that, as in our previous work [1], this is occasionally a convenient quantity to work with.

A. Critical coupling

A glance at the oscillations in Fig. 1 shows an important property of the system: the coupled elements switch in sequence so that while one element is carrying out the transition from one stable state to the other, the remaining elements are approximately at rest in one of their stable steady states. In fact, the dynamics introduces a *de facto* separation of time scales, this behavior being a result of the unidirectional coupling. Note, also, the "antiferromagnetic" configuration of the elemental state points: for odd N there is always one "frustrated" element that tries to align itself in opposition to its forward-coupled neighbor, and this generates a soliton-like ripple that transits the ring. For large arrays this behavior is quite striking [7] and includes some novel effects that arise in the presence of background noise. The oscillatory behavior can also be observed for N even and large [7].

The above separation of time scales can be exploited to determine important parameters in the vicinity of the critical point. We start with a calculation of the critical coupling

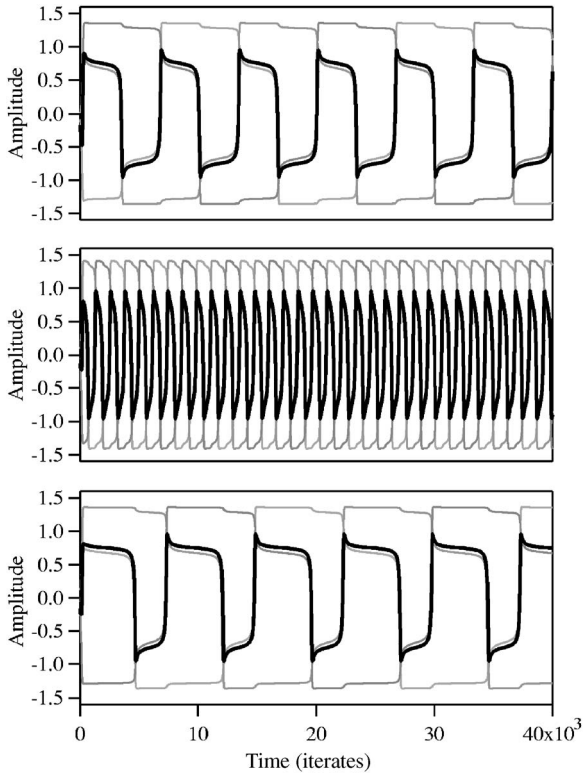

FIG. 1. Emergent oscillatory behavior in the coupled system (1) for $N=3$. The top panel shows the oscillations just past the critical point. The summed response is indicated by thick black lines (in all panels), and the individual element responses follow the gray lines in all panels. The amplitudes are fully grown at the start of the oscillations and the frequency is low (at the critical point, the frequency is zero). The middle panel shows the oscillations for a higher coupling strength. Contrasted with the top panel, the frequency increases significantly. Note that $\varepsilon_0=0$ in the first two panels. The bottom panel shows the individual element oscillations for the same parameter values as the first panel, but with $\varepsilon_0=0.1$; the (ε_0-induced) reduction in the oscillation frequency and the occurrence of unequal residence times (measured as the difference between the widths of each half-cycle, as measured at the crossing points on the horizontal axis) are both evident. Parameters $(a,b,\tau)=(53.166,57.426\ (\mathrm{C/m^2})^{-2},1.211\times10^{-5}\ \mathrm{s})$, which are parameter values measured from a BZT ferroelectric material used in a preliminary experimental realization of a coupled-element device that obeys the dynamics (1), lead to an energy barrier height of $U_0=\frac{a^2}{4b}=12.30$ so that $\varepsilon_0=0.00813U_0$. The critical coupling (for $\varepsilon_0=0$) is $\lambda_{c0}=a/2$ (see text), $\lambda=27.0$ (top and bottom panels), and $\lambda=31.0$ (center panel).

constant λ_c, setting $\tau=1$ as long as we are discussing dc target signals, only; when discussing a situation involving time-periodic signals, however, the device bandwidth τ^{-1} will become far more important. Assume that the element $x_1(t)$ is switching states, while the other two elements remain in their stable steady states. It is also clear from the above discussion that the element that $x_1(t)$ is forward coupled to [in this case $x_2(t)$] will be in the steady state that is nearly identical to the one from which the active element, $x_1(t)$, begins its switch. We can, then, "decouple" the active element from the others, writing its dynamics as

$$\dot{x}_1(t) = (a+\lambda)x_1 - bx_1^3 - \lambda x_{2m} + \varepsilon_0 \equiv f(x_1), \tag{2}$$

x_{2m} being the steady-state value of x_2. We can write the above dynamics as a gradient system, with the potential function given by

$$U(x_1) = -\frac{1}{2}(a+\lambda)x_1^2 + \frac{b}{4}x_1^4 + (\lambda x_{2m} - \varepsilon_0)x_1. \tag{3}$$

It is most important to realize that the coupled dynamics (1) *cannot* be represented as a potential system, due to the unidirectional coupling. However, during the oscillation half-cycle when a particular active element (e.g., x_1 above) is transiting the energy barrier with the other two elements taken to be approximately at rest, we can represent the evolution of the active element by the particle-in-a-potential paradigm only through this half-cycle. Then, the critical coupling corresponds to the appearance of an inflection point x_{1c} in $U(x_1)$—i.e., $U''(x_{1c})=0$ (the prime denotes differentiation with respect to x_1). This yields $x_{1c}=\pm\sqrt{\frac{a+\lambda_c}{3b}}$, which is substituted into the first derivative equation $U'(x_{1c})=0$, yielding the following equation for λ_c:

$$\frac{2}{3}\frac{(a+\lambda_c)^{3/2}}{(3b)^{1/2}} + \varepsilon_0 = \lambda_c x_{2mc}, \tag{4}$$

which has to be solved for λ_c after first determining the steady-state value x_{2mc} (at the critical coupling λ_c). The latter is accomplished by noting that x_{2mc}, being a steady-state value of the state point x_2, satisfies $U'(x_{2mc})=0$ (for a given coupling λ), where U is now taken as the potential energy function of the x_2 dynamics, the prime denotes differentiation with respect to x_2, and it is noted that $x_{3m}=-x_{2m}$. The equation for x_{2mc} is, then, found to be $(a+2\lambda)x_{2mc}-bx_{2mc}^3+\varepsilon_0=0$. For the special case of $\varepsilon_0=0$, this leads to $x_{2m0}=\pm\sqrt{\frac{a+2\lambda}{b}}$, with the subscript 0 denoting the quantity in the absence of the target signal. Substituting in the original equation (4) with $\varepsilon_0=0$ immediately yields the relevant root $\lambda_{c0}=\frac{a}{2}$.

It is, now, necessary to compute the critical coupling λ_c for a nonzero target signal. For small ε_0, we may set

$$\lambda_c = \lambda_{c0} + \delta_1,$$

$$x_{2m} = x_{2m0} + \delta_2. \tag{5}$$

Substituting these expansions into the critical point, Eq. (4), and expanding to $O(\delta_i), i=1,2$, we get, after some calculations, the following expression:

$$x_{2m} = \sqrt{\frac{a+2\lambda}{b}} + \frac{\varepsilon_0}{2(a+2\lambda)}, \tag{6}$$

for arbitrary coupling strength λ, whence λ_c is found by setting $\lambda=\lambda_c$ in Eq. (6) (this yields x_{2mc}) and using the first of the expansions (5) in Eq. (4). Then, after some calculations, we obtain

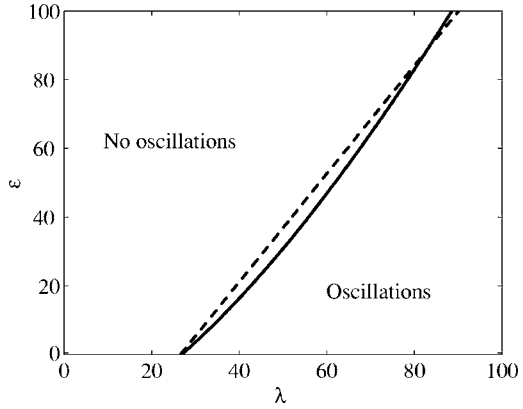

FIG. 2. For the dc target signal case, there are only two distinct regimes of behavior. To the left of the critical coupling there is no oscillation. To the right of the critical coupling, the elements oscillate out of phase by $2\pi/3$ ($2\pi/N$ in general) from each other but with the same amplitudes and frequencies. The analytical result given by (7) (dashed line) and the numerical result (solid line) obtained by direct simulation of (1) agree quite well even in regimes wherein the low-ε_0 approximation is not applicable. System parameters as in Fig. 1.

$$\lambda_c = \lambda_{c0} + \frac{3}{2}\frac{\varepsilon_0}{1+\sqrt{\frac{2a}{b}}}, \tag{7}$$

to leading order in ε_0. This expression for the critical coupling is found to agree quite well with the results of numerical simulations on the coupled system (1) for small (compared to the energy barrier height U_0) ε_0 (Fig. 2).

B. Oscillation period

We now turn to a more detailed description of the dynamics of (1), confining ourselves to the immediate neighborhood of the critical point in the oscillatory regime—i.e., when the separation $\lambda_c-\lambda$ is small. We note, however, that our results provide a very good qualitative description of the dynamics (in particular, the scaling of the oscillation period with the coupling strength and/or symmetry-breaking signal) well past the onset of the oscillations; this was already observed in our previous work [1]. We carry out the analysis for $N=3$ elements; the generalization to arbitrary N will be made clear at the end. We refer to Fig. 1, specifically the third panel in which we have shown the summed response $X(t)=\Sigma_i x_i(t)$, having period T_+. It is clear, from this figure, that the zero crossing points t_0 $(=0), t_1, t_2$, etc., of the summed output $X(t)$ also correspond to the crossing points of the individual elemental solutions $x_i(t)$. Hence, the problem of finding the period T_+ of the summed output reduces to determining the zero-crossing times $t_{1,2}(t)$.

We exploit the previously discussed property that, near the bifurcation point, the elements evolve (approximately) individually so that the evolution of $x_1(t)$ can be described by the reduced dynamics (2). The first crossing point of this solution, on the t axis, can be obtained from

$$t_1 = \int_{x_+}^{0} \frac{dx_1}{f(x_1)}.$$

The integral may be simplified by first interchanging the limits and then noting that the integrand $-1/f(x_1)$ is sharply peaked at $x_1=x_{10}=\sqrt{\frac{a+\lambda}{3b}}$, where we take the positive sign for the square root because x_1 starts from a positive steady state x_+; of course, the treatment and results are independent of the particular choice of initial states, as long as at least one element is not in the same initial state as the others. We then Taylor expand the denominator about x_{10} and carry out the integration after first extending the limits to $\pm\infty$. These approximations hold very well in the neighborhood of the critical point. The result, after some tedious algebra, is

$$t_1 = \frac{\sqrt{2}\pi}{\sqrt{|f(x_{10})f''(x_{10})|}},$$

in which all the quantities in the denominator can easily be calculated. The next crossing point is obtained by considering, for instance, the evolution of $x_3(t)$ from its (negative) steady state $x_{30}=-x_{10}$ to the t axis, while x_1 remains in its steady state $x_{1m}=-x_{2m}$. Carrying out the same steps as before, we obtain, for the *interval* t_{12},

$$t_{12} = \frac{\sqrt{2}\pi}{\sqrt{|f(x_{30})f''(x_{30})|}},$$

so that the summed oscillation period is written as

$$T_+ = t_1 + t_{12}. \tag{8}$$

It is easy to see that the period of each individual oscillation is $T_i=3T_+$ (in general, this would be NT_+) and the phase difference between individual oscillations is $2\pi/3$ ($2\pi/N$ in general). Increasing N leads to a concomitant increase in the individual oscillation periods, but the period of the summed response is independent of N. The residence times difference in the two states is easily evaluated, via the summed response, as $\Delta t=t_1-t_{12}$; note that the quantity Δt would incorporate a factor of N if we evaluated it for each individual element. We also point out that, unlike in our previous work [1], it does not appear possible to (analytically) obtain a clear-cut scaling behavior of the period T_+ with the "separation" $\Delta\lambda\equiv\lambda-\lambda_c$ from the expressions above; in fact, the necessity to recourse to Taylor expansions for the steady-state quantities x_{i0} as well as the critical coupling λ_c attests to the calculational difficulties associated with this (seemingly straightforward, especially in comparison to the more complicated mean-field potential energy functions of [1]) coupled system (1), even near the critical point. It is possible, however, to compare the oscillation frequency obtained theoretically with the results of repeated numerical simulations of the dynamics (1) for different values of the bifurcation distance $\lambda-\lambda_c$. This is shown in Fig. 3 wherein we also show the (very good) fit obtained to a $(\lambda-\lambda_c)^{1/2}$ scaling law, in line with our previous work on the coupled ferromagnetic system [1]. It is also clear that for small (as defined in Fig. 1) ε_0, the theoretical predictions match the simulation results quite well.

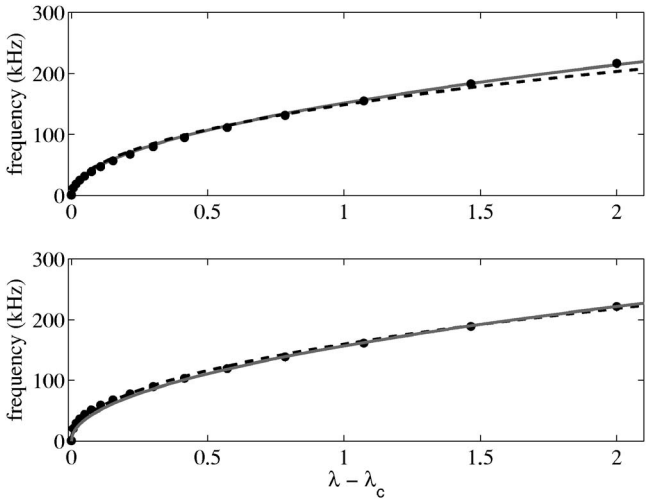

FIG. 3. The (summed) oscillation frequency obtained via the theoretical expression (8) (dashed curve) and direct numerical simulations of the coupled system (1) for $\varepsilon_0=0$ (top) and 0.1 (bottom). The agreement is seen to be quite good. The numerical fits (solid curves) to the scaling laws $f=151.631(\lambda-\lambda_c)^{1/2}$ (top) and $f=156.904(\lambda-\lambda_c)^{1/2}$ (bottom) are also shown. Other system parameters are as in Fig. 1.

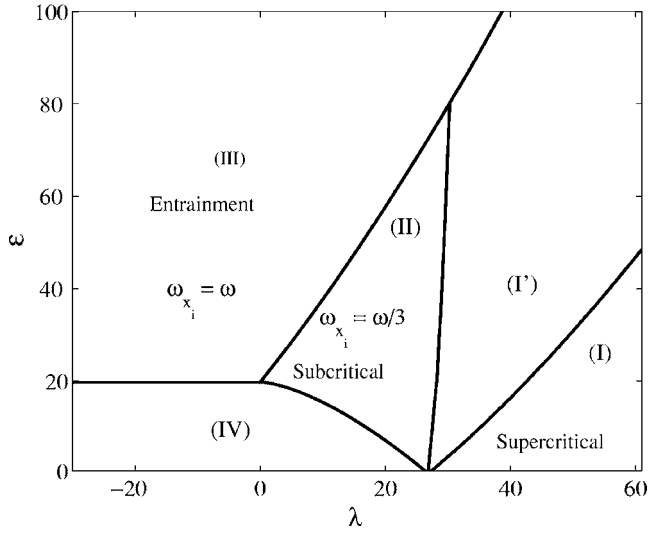

FIG. 4. Different oscillatory regimes (via numerical simulations) for $N=3$ locally coupled overdamped Duffing elements subject to an ac target signal. (I) Supercritical regime: coupled system oscillates in a traveling wave pattern; i.e., individual wave forms are out of phase by $2\pi/3$. (I′) Intermittency: each Duffing system exhibits periodic excursions between oscillatory solutions and equilibrium points. (II) Subcritical regime: oscillatory solutions whose frequencies are locked to the subharmonic target frequency $\omega/3$. (III) Entrainment regime: complete frequency and phase synchronization with target signal. (IV) No oscillations. System parameters as in Fig. 1.

III. THE CASE OF A TIME-PERIODIC TARGET SIGNAL

Multistability and the response of deterministic nonlinear dynamic systems to time-periodic excitations have been studied in the literature [8,9]. It has been observed that the dynamical hysteresis loop of the system response has an area that scales as the two-thirds power of the frequency of the excitation signal. The switching (from one stable branch of the hysteresis loop to the other) experiences a "delay," i.e., a larger value of the control parameter is required in order to induce switching, when the driving signal is time periodic. In our earlier work [5] on coupled ferromagnetic cores, we observed related behavior. Specifically, we constructed a phase diagram wherein at least three distinct regimes of behavior (each defined by the value of the coupling coefficient in relation to its critical value) wherein one could obtain system oscillations at multiples (or subharmonics) of the applied frequency, even in the so-called subcritical regime characterized by a coupling coefficient, such that no spontaneous oscillations (in the absence of the applied target signal) were possible.

We now apply a time-periodic external signal $\varepsilon \sin \omega t$ with a controllable amplitude and frequency to the system (1). Then, a phase diagram (with λ and ε as control parameters) can be constructed to characterize the response [measured via the oscillation frequency of each solution $x_i(t)$] of the driven coupled system. This diagram is shown in Fig. 4. One immediately observes the following distinct regimes of behavior: (I) supercritical regime, wherein the coupled system oscillates in a traveling-wave pattern with similar characteristics to the oscillations found for the case of a dc external signal (Fig. 2); (I′) intermittent regime, wherein the collective pattern of behavior shows intermittency in which each individual element of (1) periodically switches between oscillatory behavior and equilibrium points; (II) subcritical regime, wherein the coupled system exhibits oscillatory solutions whose frequencies are locked to the subharmonic frequency $\omega/3$; (III) entrainment regime characterized by a complete synchronization of amplitudes, phases, and frequencies of each individual element with each other and their frequencies are locked to the target signal's frequency; and (IV) a regime wherein no oscillatory behavior is observed. The three regimes of oscillation intersect at a dynamical "triple point" The terms "supercritical" and "subcritical" as applied to Fig. 4 deserve some clarification. Note that the boundary between regions (I) and (I′) corresponds to the solid curve in Fig. 2, with the subcritical and supercritical regimes defined with reference to this curve (i.e., as defined for the dc target signal case) for consistency. Clearly, the nonoscillating regime of Fig. 2 gives way to substantially modified (and enriched) behavior in the presence of the ac target signal. Finally, we note that, for sufficiently large signal amplitudes, one can obtain oscillations locked to the applied frequency, even in the absence of coupling; this is, of course, well known and it is referred to as the overdriven case.

It is, clearly, of some interest to further quantify the regimes in this phase diagram; specifically, we are interested in the equations of the curves that emanate from the triple point and delineate the different dynamical regimes. We begin by computing the critical signal amplitude ε_c, which suffices to introduce switching in the coupled system, given some values of the coupling coefficient and signal frequency. We address this question through the entirety of the dynamic equa-

tions (1) taking (unlike the previous section) the device time constant τ to be finite. In the presence of an externally imposed time scale (the signal period), this time constant becomes important in the description of the system response; specifically, we will see that the critical amplitude ε_c is a function of τ. Our calculation is based on the earlier calculation of Jung *et al.* [8]. It is convenient to rescale time by introducing the variable $t=\tau s$, thereby transforming the system (1) into

$$\dot{x}_i = ax_i - bx_i^3 + \lambda(x_i - x_{i+1}) + \varepsilon \sin(\omega\tau s), \tag{9}$$

where $i=1,\ldots,N$ mod N, the overdot now denotes the derivative with respect to s. Once again, we can exploit the fact that the coupled elements evolve one at a time, so that the evolution of x_1 can be written as

$$\dot{x}_1 = (a+\lambda)x_1 - bx_1^3 + \lambda x_{2m} + \varepsilon \sin(\Omega s), \tag{10}$$

where $\Omega=\omega\tau$ and x_{2m} is given by Eq.(6). We now expand Eq. (10) about the critical point $x_-=-\sqrt{\frac{a+\lambda}{3b}}$, obtaining the following equation for the (small) deviation from this critical point; i.e., we write $x=x_-+y$, having dropped the suffixes for convenience:

$$\frac{dy}{ds} = \sqrt{3(a+\lambda)b}y^2 - by^3 + \lambda x_m - F_0 + \varepsilon \sin(\Omega s), \tag{11}$$

with $F_0=\sqrt{\frac{4(a+\lambda)^3}{27b}}$ and $x_m=x_{2m}$. Setting $F(s)=F_0-\lambda x_m + E\sin(\Omega s)$, where $E^2=\varepsilon^2-(F_0-\lambda x_m)^2$, we obtain

$$\frac{dy}{ds} = \sqrt{3(a+\lambda)b}y^2 - O(y^3) + E\sin(\Omega s). \tag{12}$$

Equation (12) is solved by first converting it into a Mathieu equation via the transformation $y(s)=[3(a+\lambda)b]^{-1/2}du/ds$ and taking the low frequency limit $\Omega\to 0$. The solution, in terms of Airy functions, is given by

$$y(s) = \sigma^{2/3}E\Omega\frac{\mathrm{Ai}'[-\sigma^{2/3}\sqrt{3(a+\lambda)b}E\Omega s]}{\mathrm{Ai}[-\sigma^{2/3}\sqrt{3(a+\lambda)b}E\Omega s]}, \tag{13}$$

where we define $\sigma^2=[3(a+\lambda)b]^{-1}\Omega^2E^2$ and the prime denotes differentiation with respect to the argument. From this, it is easy to write down the delayed value of the bifurcation parameter, F_{del} in terms of the zero-argument Airy function:

$$F_{del} = (F_0 - \lambda x_m) + \left[\frac{(\Omega E)^2}{\sqrt{3(a+\lambda)b}}\right]^{1/3}\left[\frac{\mathrm{Ai}'(0)}{\mathrm{Ai}(0)}\right]^2, \tag{14}$$

which, finally, takes the form

$$F_{delay} = (F_0 - \lambda x_m) + k_1\{\Omega^2[\varepsilon^2 - (F_0 - \lambda x_m)^2]\}^{1/3}. \tag{15}$$

The critical amplitude occurs when $\varepsilon_c=F_{delay}$, which yields

$$\varepsilon_c = (F_0 - \lambda x_m) + k_1\{\Omega^2[\varepsilon_c^2 - (F_0 - \lambda x_m)^2]\}^{1/3}, \tag{16}$$

where k_1 is a fit parameter that is a function of a, b, λ, and Ω. Also note the $\Omega^{2/3}$ dependence of the critical amplitude; this behavior is in line with earlier results [8,9] on the behavior of the hysteresis loop in a "soft" material that is subjected to a time-periodic excitation. The three roots for ε_c in Eq. (16) are

$$\varepsilon_c = \frac{F_0 - \lambda e}{1+\lambda f},$$

$$\varepsilon_c = \frac{2(F_0-\lambda e)(1+\lambda f) + k_1^3(1-\lambda f)\Omega^2}{2(1+\lambda f)^2} \pm \frac{\sqrt{k_1^3\Omega^2[8(F_0-\lambda e)(1+\lambda f) - k_1^3\Omega^2(1-\lambda f)]}}{2(1+\lambda f)^2}, \tag{17}$$

where $e=\sqrt{(a+2\lambda)/b}$ and $f=1/[2(a+2\lambda)]$. The first solution delineates the nonoscillatory regime from the $\omega/3$ oscillatory regime for $0<\lambda<\lambda_0$. Notice that this solution (separation line) is frequency independent so that the separation will hold true for $\omega\geqslant 0$. The two conjugate solutions are dependent on the frequency of the time-periodic signal. One of the solutions sets the boundary separating the $\omega/3$ regime from the other oscillatory behaviors for $\lambda\geqslant\lambda_0$. Figure 4 illustrates these behaviors through the solutions of Eqs. (17). The two conjugate solutions can have imaginary parts; however, we require that the coupling constant cannot have an imaginary part in order to make physical sense; in turn, this demands that the radicant must be equal or greater than zero. Using this condition we get a lower bound on k_1 given by

$$k_1 \geqslant \frac{2[(\lambda e - F_0)(1+\lambda f)]^{1/3}}{(\lambda f - 1)^{2/3}\Omega^{2/3}} = 2\beta. \tag{18}$$

The lines plotted in Fig. 5 use $k_1=3\beta$ so that we can get the best fit between the numerical results and the analytical approximations in Eqs.(17)

Next there is a line that separates the $\omega_{xi}=\omega/3$ regime from the entrainment regime where $\omega_{x_i}=\omega$. An analytical expression can be found by finding an approximate solution near the point at $\lambda=0$. We note that, for a strong amplitude

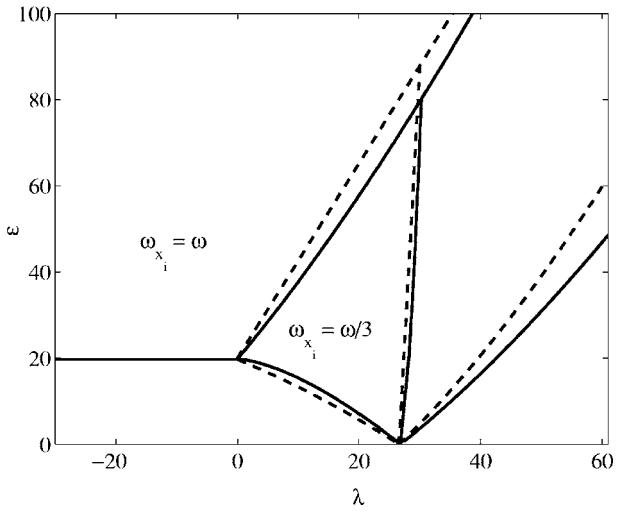

FIG. 5. Comparison of analytical (dashed lines) and numerical (solid lines) boundary curves that separate the different oscillatory regimes in parameter space (λ,ε), for $N=3$ elements in (1). System parameters as in Fig. 1.

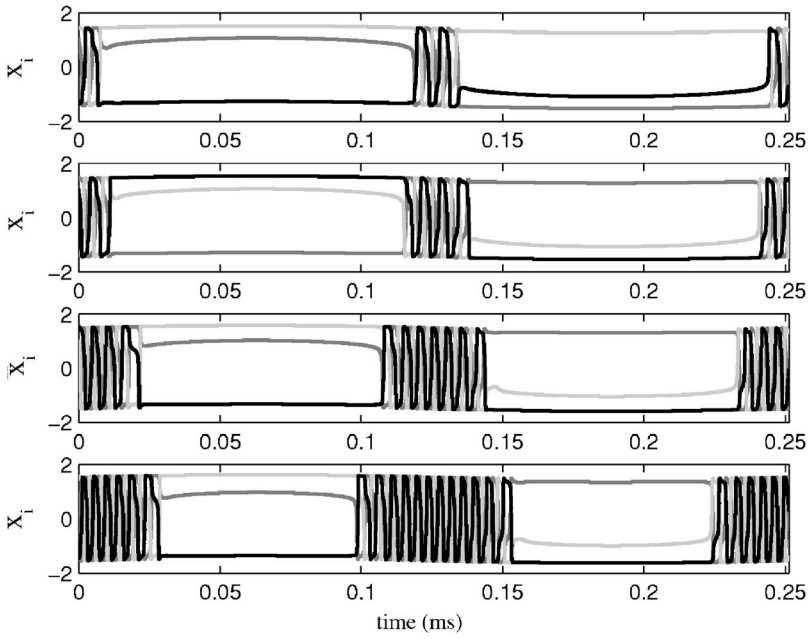

FIG. 6. Intermittent behavior found in region (I′) of Fig. 4. The individual solutions $x_i(t)$ of (9) are plotted. As λ increases, the switching events last longer until the resulting intermittent pattern coalesces with the traveling-wave pattern of the supercritical regime. $\lambda=33,35,39,43$ (top-to-bottom panels), $\varepsilon=30$, $\omega=25000$. Other parameters as in Fig. 1. Note that each element x_i displays alternate "slow" and "fast" oscillations.

signal, the coupled system oscillates in synchrony with identical phases and amplitudes among the three elements. We can use this fact to calculate an analytical expression for the onset of this synchronous oscillatory behavior. The calculation is easier if we transform the dynamical equations (1) into the amplitude and phase equations. This yields, for $N=3$, the system

$$\dot{r}_1 = (1-r_1^2)r_1 + \hat{\lambda}(r_1 - r_2\cos\phi_1) - \hat{\varepsilon}e\sin\theta_1,$$

$$\dot{r}_2 = (1-r_2^2)r_2 + \hat{\lambda}(r_2 - r_3\cos\phi_2) - \hat{\varepsilon}e\sin\theta_2,$$

$$\dot{r}_3 = (1-r_3^2)r_3 + \hat{\lambda}(r_{-3} - r_1\cos\phi_3) - \hat{\varepsilon}e\sin\theta_3,$$

$$\dot{\theta}_1 = -\hat{\omega} - \hat{\lambda}\frac{r_2}{r_1}\sin\phi_1 - \frac{\hat{\varepsilon}e}{r_1}\cos\theta_1,$$

$$\dot{\theta}_2 = -\hat{\omega} + \hat{\lambda}\frac{r_3}{r_2}\sin\phi_2 - \frac{\hat{\varepsilon}e}{r_2}\cos\theta_2,$$

$$\dot{\theta}_3 = -\hat{\omega} - \hat{\lambda}\frac{r_1}{r_3}\sin\phi_3 - \frac{\hat{\varepsilon}e}{r_3}\cos\theta_3, \tag{19}$$

where r_i is the averaged amplitude over one period of the ac signal, $\hat{\omega}=\omega\tau/a$, $\hat{\lambda}=\lambda/a$, $\hat{\varepsilon}=\varepsilon-\varepsilon_0$, $e=1/[a\sqrt{4a/(3b)}]$, $\phi_1=\theta_2-\theta_1$, $\phi_2=\theta_2-\theta_3$, and $\phi_3=\theta_1-\theta_3$; ε_0 is the critical external signal amplitude to cause the entrainment in region III for zero coupling and its value can be calculated using the first root in Eq. (17) when $\lambda=0$. Furthermore, by assuming the radial components $r_{j's}$ to be identical, the amplitude-phase equations (19) reduce to

$$\dot{r}_j = (1-r_j^2)r_j + \hat{\lambda}(r_j - r_j\cos\phi_j) - \hat{\varepsilon}e\sin\theta_j,$$

$$\dot{\phi}_j = 2\hat{\lambda}\sin\phi_j + 2\hat{\lambda}e\sin\frac{\Sigma_j}{2}\sin\frac{\phi_j}{2},$$

$$\dot{\Sigma}_j = -2\hat{\omega} - 2\hat{\varepsilon}e\cos\frac{\Sigma_j}{2}\cos\frac{\phi_j}{2}, \tag{20}$$

where $\Sigma_j=\theta_j+\theta_{j+1}$, $j=1,\ldots,N \bmod N$. From Eqs.(20), we observe that the synchronized state corresponds an equilibrium point of the form $p^*=(r^*,\phi_j=0,\Sigma_j^*)$, where r^* denotes a non-negative amplitude state while Σ_j^* denotes a nonzero sum-phase variable. Linearizing Eqs.(20) about p^*, we find the eigenvalue along the ϕ_j direction to be $\sigma_\phi=2\lambda/a-(\varepsilon-\varepsilon_0)\sqrt{3b/(4a)}/a$. The synchronized state emerges when $\sigma_\phi=0$, yielding the marginal stability curve

$$\varepsilon = \varepsilon_0 + 2\lambda\sqrt{\frac{4a}{3b}}. \tag{21}$$

Figure 5 illustrates the analytical (dashed lines) boundary curves, which separate the different oscillatory regimes, defined by Eqs.(7), (17), and (21). The numerically obtained boundaries (solid lines), previously shown in Fig. 4, are also included to highlight the good agreement between analytical results and numerics.

We conclude this section with a few comments about the intermittent behavior that appears in region (I′) of Fig. 4. We set the parameters (ε,λ) within region (I′), then fix ε and vary λ so that we can traverse the two-parameter bifurcation diagram of Fig. 4 across the intermittent regime (I′). Numerical simulations (Fig. 6) show that near the boundary of the subcritical region (I), each element will periodically switch, for a brief period of time, between its allowed (stable) steady states. As the coupling strength λ increases, the back and forth excursions between equilibrium points become increasingly rapid (with a concomitant decrease in the duration of the "slow" oscillations) until λ is large enough for the switching events to occur continuously, at

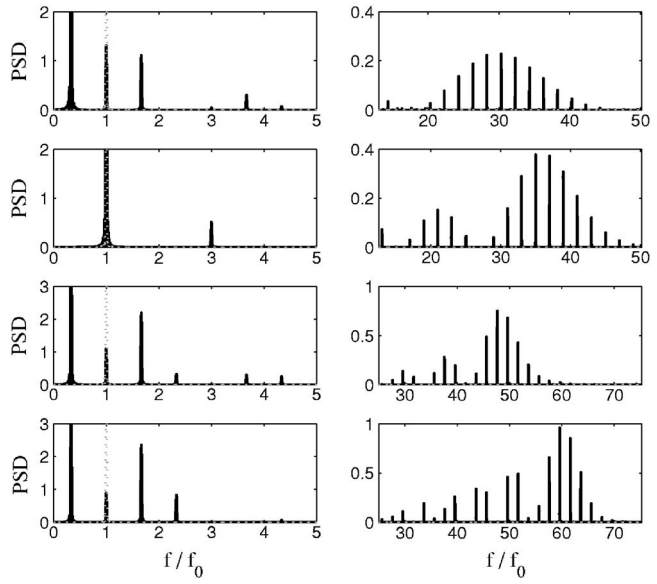

FIG. 7. Power spectra for one solution computed for each of the cases of Fig. 6. The frequency scale is normalized to the applied signal frequency f (=3.9789 kHz). Left and right panels show spectra at low and high frequencies for each case.

which point we have crossed into the supercritical regime. From a dynamical systems point of view, the observed intermittent behavior results from the periodic perturbation by the ac target signal of the heteroclinic cycle that exists in the coupled Duffing system when the target signal only has a dc component. Figure 7 shows the power spectra obtained for any single solution at low and high frequencies; each two-panel row corresponds to the same panel in Fig. 6, with the frequency axis normalized to the applied signal frequency (f=3.9789 kHz). It is clear that control parameter λ sets the relative peak heights. For panels 1, 3, and 4 (top to bottom), the peaks occur at multiples $nf/3$ (n odd) of the applied frequency. We reiterate that some peaks are not visible on the scale of the figure; this is particularly apparent in the second (from top) panel wherein the (visible) peaks are at nf (n odd) and the remaining peaks in this sequence all but suppressed (although they do occur) for this value of λ. The nonoccurrence of peaks at even multiples of the impressed frequency may be traced (in the *absence* of coupling) to the symmetry of the underlying dynamics, specifically the nonlinearity $f(x_i)=ax_i-bx_i^3$. For odd $f(x_i)$, one can show that the power spectral density will contain the odd multiples of $f/3$. In a potential system, this would correspond to an *a priori* symmetric potential energy function. When the underlying symmetry is broken (e.g., by the inclusion of a dc component in the external driving term), the result is the appearance of all the harmonics nf (n an integer). In Fig. 7, however, it is observed that the coupling modifies the above selection rules, since the only external signal present is the time-sinusouidal signal $\varepsilon \sin \omega t$. It can be verified (not shown) that, with an additional small dc offset ε_0, panels 1, 3, and 4 contain peaks at $nf/3$ and panel 2 contains peaks at nf (n an even or odd integer in both cases). The appearance of these specific sequences of harmonics and subharmonics of the applied frequency in this particular regime is, therefore, a subject that would bear further investigation.

IV. DISCUSSION

The current work indicates that, while one can expect rich dynamical behavior (in this case, the generation of oscillations past a critical point) in a wide class of nonlinear dynamic elements, it would be a mistake to assume that standard solutions exist for all forms of the nonlinearity. Our previous work [1] dealt with coupled ferromagnetic cores with a mean-field type of nonlinearity; in turn, this rendered the dynamics seemingly more complicated with the coupling and external forcing terms incorporated inside the nonlinearity due to the mean-field nature of the magnetic dynamics, as already noted earlier. However, the scaling of the oscillation frequency with $(\lambda-\lambda_c)^{1/2}$ that was observed in the coupled ferromagnetic cores subject to a dc target signal ε_0 is also present in the system at hand.

The present system shows some interesting phenomena. The appearance of a "triple point" in the phase diagram when a time-cyclic signal is applied provides food for thought. While a broad theoretical treatment of this point does not yet exist, it is intriguing to ponder its significance: for one unique value of the amplitude of the time-periodic driving signal, one could have three different regimes of oscillations with only miniscule changes in the coupling parameter.

Despite all the above issues and caveats, the real importance of this work is embodied in its applicability to a number of actual dynamical systems and devices. In particular, as already noted, a detector for changes in the ambient electric field can be constructed by coupling ferroelectric material samples in this manner and observing the oscillation characteristics of the resulting electric field sensor. The experiments (to be described in an upcoming publication) are the very first of their kind, and the coupling-induced oscillations in the polarization of each ferroelectric are central to this device. In fact, the system parameters (a,b,τ), used in the numerical simulations throughout this paper (see Fig. 1 caption for the values), were obtained through the laboratory characterization of a $BaZr_xTi_{1-x}O_3$ (BZ) ferroelectric sample used in our experiments. In practice, the polarization oscillations are transduced into a voltage [10], which is readily measurable. The typical ferroelectric material has a prohibitively large coercive field [11] so that using a single-element sensor as an electric field detector would necessitate a very large onboard reference signal to preexcite transitions between the stable states of the transfer characteristic before a small target signal could be detected via its asymmetrizing effects on the dynamics; in turn, this is likely to require a prohibitively large onboard power supply as well as generate a significant noise floor in the measurement. This problem is not present in the fluxgate magnetometer which can readily be realized as a single-core device [2,12]. Clearly, for the system at hand, these problems are mitigated via the coupling, since the dynamics provide the necessary transitions between the steady states of each elemental transfer characteristic. Accordingly, unlike the coupled-core fluxgate magnetometer of our previous work [1], a detector that is supposed to quantify changes in the ambient electric field *onboard the sensor* (i.e., without measuring a voltage drop across electrodes implanted in the active medium) can be conveniently realized as a coupled system of the form considered in this work. We

also make the point that in any practical realization, the coupling circuitry does require some onboard power, so that the occurrence of the oscillations does not violate any fundamental laws.

It should be quite clear that the unidirectional coupling scheme can lead to new vistas of dynamical behavior. This behavior can be exploited for practical applications as shown in our work to date. However, some practical issues—e.g., a detailed quantification of the effects of a noise floor [13] and variations on the basic coupling scheme [7] (to include large N, odd and even N, and ferromagnetic or antiferromagnetic coupling)—have been addressed in only a preliminary way; these will be the focus of subsequent publications.

ACKNOWLEDGMENTS

The authors acknowledge support from the Office of Naval Research (Code 331). P.L. and A.P. were supported in part by U.S. Space and Naval Warfare Systems Command, Grant No. N66001-06-M-108.

[1] A. R. Bulsara, V. In, A. Kho, W. Rappel, J. Acebron, A. Palacios, P. Longhini, S. Baglio, and B. Ando, Phys. Rev. E **70**, 036103 (2004).

[2] A. R. Bulsara, C. Seberino, L. Gammaitoni, M. Karlsson, B. Lundqvist, and J. Robinson, Phys. Rev. E **67**, 016120 (2003).

[3] V. In, A. Kho, J. D. Neff, A. Palacios, P. Longhini, and B. Meadows, Phys. Rev. Lett. **91**, 244101 (2003).

[4] A. Palacios, R. Carretero-Gonzales, P. Longhini, N. Renz, V. In, A. Kho, J. Neff, B. Meadows, and A. R. Bulsara, Phys. Rev. E **72**, 026211 (2005).

[5] V. In, A. R. Bulsara, A. Kho, P. Longhini, and A. Palacios, Phys. Rev. E **72**, 045104(R) (2005).

[6] See, e.g., H. E. Stanley, *Introduction to Phase Transitions and Critical Phenomena* (Oxford University Press, Oxford, 1971).

[7] J. Lindner and A. Bulsara (unpublished).

[8] P. Jung, G. Gray, R. Roy, and P. Mandel, Phys. Rev. Lett. **65**, 1873 (1990).

[9] T. Tome and M. J. de Oliveira, Phys. Rev. A **41**, 4251 (1990); M. Rao, H. R. Krishnamurthy, and R. Pandit, Phys. Rev. B **42**, 856 (1990); B. Chakravarty and M. Acharya, Rev. Mod. Phys. **71**, 847 (1999); H. Fujisaka, H. Tutu, and P. A. Rikvold, Phys. Rev. E **63**, 036109 (2001).

[10] S. Sivasubramanian, A. Widom, and Y. Sristava, IEEE Electr. Insul. Mag. (USA) **50**, 950 (2003).

[11] M. Lines and A. Glass, *Principles and Applications of Ferroelectrics and Related Materials* (Oxford University Press, New York, 1977).

[12] B. Ando, S. Baglio, A. Bulsara, and V. Sacco, IEEE Sens. J. **5**, 895 (2005); IEEE Trans. Instrum. Meas. **54**, 1366 (2005).

[13] A. Bulsara, J. Lindner, V. In, A. Kho, S. Baglio, V. Sacco, B. Ando, P. Longhini, A. Palacios, and W.-J. Rappel, Phys. Lett. A **353**, 4 (2006).